Single-mask microfabrication of three-dimensional objects from strained bimorphs

2007 J. Micromech. Microeng. 17 N63

(http://iopscience.iop.org/0960-1317/17/9/N01)

IOP Publishing Journal of Micromechanics and Microengineering
J. Micromech. Microeng. **17** (2007) N63–N68 doi:10.1088/0960-1317/17/9/N01

NOTE

Single-mask microfabrication of three-dimensional objects from strained bimorphs

E Moiseeva, Y M Senousy, S McNamara and C K Harnett

Department of Electrical and Computer Engineering, 248 Belknap Research Building, University of Louisville, Louisville, KY 40208, USA

E-mail: c0harn01@gwise.louisville.edu

Received 16 May 2007, in final form 6 July 2007
Published 17 August 2007
Online at stacks.iop.org/JMM/17/N63

Abstract
Recently, techniques known as 'micro-origami' or 'strain architecture' have emerged for the fabrication of out-of-plane micro- and nanostructures by relaxation of a pair of strain-mismatched thin films. Applications of such structures include optical reflectors, actuators and micropositioners. We illustrate how control of the folding order can generate complex three-dimensional objects from metal-oxide bilayers using this approach. By relying on the fact that narrower structures are released from the substrate first, it is possible to create multi-axis loops and interlinked objects with several sequential release steps, using a single photomask. The structures remain planar until released by XeF_2 dry silicon etching, making it possible to integrate them with other MEMS and microelectronic devices early in the process.

1. Introduction

Layered sheets of materials with mismatched strain will roll up with a well-defined radius of curvature, a principle which has long been used in macroscopic systems such as bimetallic thermometer coils. Recently, however, researchers have applied this strained-bimorph principle to thin film bilayers at much smaller scales, using epitaxially grown semiconductor films to produce coiled cantilevers and tubes with internal radii down to 2 nm [1–5]. Metal/semiconductor systems have been used to produce nanoscrolls with radii less than 500 nm [6]. These research efforts demonstrate an elegant method, known as 'micro-origami' or 'strain architecture,' to fabricate out-of-plane micro- and nanostructures that would not be possible with conventional planar lithography. Although strain architecture can be considered a self-assembly method, it differs from the stochastic nature of most self-assembly processes in that structures are produced in registration with each other and may be aligned with other layers on the substrate during lithography.

Out-of-plane micro- and nanostructures are desired especially in applications where microelectromechanical systems (MEMS) must interface with the external environment. For example, micro-origami has produced mirrors [5, 7], stages [8], shutters [9] and corner-cube reflectors [10] to handle optical signals, out-of-plane directed cantilevers to act as field emitters [11] and nanopipelines to handle fluids [4]. A significant fraction of micro-origami research concerns actuators, including thermal actuators [12–15], electrostatic actuators [9, 16] and chemical actuators [12]. While these actuators' typical purpose is to manipulate cells and other small objects, a very practical application is one-time-use integrated levers [17] to assemble complex MEMS systems without human intervention.

In this paper, we investigate the effect of folding order on the final shape of these three-dimensional micro-objects. We create strain mismatch by patterning a metal-on-SiO_2 layer on a silicon substrate. Thermally grown SiO_2 generally has compressive stress, while the metal films used in this work have tensile stress. The silicon is isotropically etched to undercut and release the metal-oxide bimorphs. The width of features in a single photomask determines the folding sequence, because the silicon etch process will undercut the narrowest lines first,

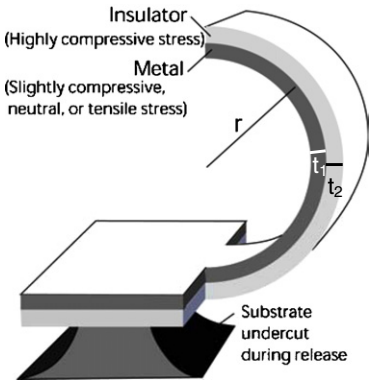

Figure 1. Schematic of a metal–insulator bimorph bending because of strain-mismatch induced curvature upon release from the substrate.

enabling those structures to curl up from the substrate before other features are released. We demonstrate that folding sequence has a large and sometimes irreversible effect on the ultimate shape of the micro-objects.

2. Theory

Strain-mismatched bimorphs attain a radius of curvature that minimizes the potential energy of the entire structure. Like a spring with stored elastic energy, a thin film that is compressively stressed while constrained to the substrate will expand when released.

A single released layer will bend only at the release point, and expand volumetrically elsewhere, resulting in a folded-over flap [4]. However, if the layer is coated with another film having less compressive stress or tensile stress, the upper film will constrain the expansion at the top of the lower film, causing the released bilayer to curl uniformly upward from the substrate. This situation is illustrated in figure 1.

Beam equations developed for much larger structures can account for most of the features seen in microscale strain-architecture devices, although the approximations become less accurate as the curvature radius becomes small relative to beam thickness [16].

For a released beam of uniform width, with no applied moments, the reciprocal of the radius of curvature is given by equation (1) [5], [18].

$$\frac{1}{\rho} = \frac{6\varepsilon(1+m)^2}{d[3(1+m)^2 + (1+mn)\{m^2 + (mn)^{-1}\}]}. \qquad (1)$$

In the above equation, ρ is the radius of curvature, d is the combined thickness of the two layers $(d_1 + d_2)$, ε is the strain mismatch or fractional difference in the unconstrained relaxed lengths of the two layers $(l_2 - l_1)/l_o$, n is the ratio of the elastic modulus of the layers (E_1/E_2) and m is the ratio of their thicknesses, (d_1/d_2). Subscripts 1 and 2 refer to the upper and lower layers, respectively. Bi-directional curvature, important even when the cantilever is narrow, can be accounted for by replacing the elastic modulus with the biaxial modulus $E' = E/(1-\nu)$, where ν is Poisson's ratio and E is the elastic modulus [19].

For many choices of materials, the biaxial moduli are similar ($n = 0.5$–2), making this parameter's effect on the radius of curvature small compared to the effects of strain mismatch and film thickness. Considerable insight can be gained by assuming that both layers have the same biaxial moduli ($n = 1$). Equation (1) then becomes

$$\frac{1}{\rho} = \frac{6\varepsilon d_1 d_2}{d^3}. \qquad (2)$$

Notably, the inverse radius is directly proportional to the strain mismatch ε, which depends upon the choice of materials and deposition conditions.

Because the minimum radius determines the lower size limit of objects that can be fabricated by this method, it is useful to extract further design rules by minimizing the reciprocal of equations (1) and (2). For two layers with equal biaxial modulus ($n = 1$) and a *fixed total thickness* d, the minimum radius occurs when the top and bottom layers have equal thicknesses ($d_1 = d_2$).

However, from a practical standpoint, oxidized wafers are typically purchased in a large batch, or oxide is grown on several wafers in one run, so the bottom layer often has a *fixed lower layer thickness* d_2, while the upper metal layer thickness d_1 is varied in subsequent processing. In this case, when both materials have equal modulus, the radius is minimized when the top layer's thickness is *half* that of the lower layer. Adding more material to the top layer only increases the total thickness d in the denominator, producing a larger radius of curvature.

In general, to minimize the radius if the biaxial moduli are unequal, the layer with the larger modulus must be thinner than the limits set by the above design rules.

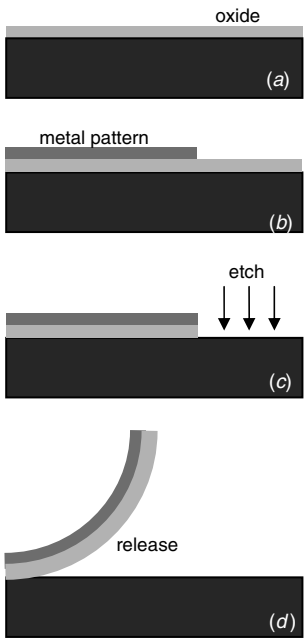

Figure 2. (*a*) Silicon wafer with 400–500 nm thermal oxide. (*b*) A 200–300 nm thick metal pattern is applied using photoresist liftoff. (*c*) The metal acts as an etch mask to pattern the oxide in a CF_4/H_2 plasma etch. (*d*) The metal-oxide bimorph is released by etching the silicon in XeF_2 gas. The oxide's compressive stress is released by curling the bimorph out of the plane.

3. Fabrication

Figure 2 illustrates the fabrication steps used to produce metal-oxide bimorphs on silicon wafers. To create a compressively

Table 1. Material properties, layer thickness, stress and calculated curvature radius for Cr–Ni–Cr/oxide and Ti–TiNi/oxide bimorph structures.

Device composition	Material	Elastic modulus (GPa)	Poisson's ratio	Measured thickness (nm)	Measured residual stress (MPa)	Calculated radius (μm)
Cr–Ni–Cr on oxide	Thermal oxide	71 [20] 83 [21]	0.20 [22]	400 ± 20	−300 ± 25 (compressive)	64 ± 7
	Cr	140 [16]	0.21 [23]	Combined metal film 160 ± 20	Combined 775 ± 50 (tensile)	
	Ni	210 [14] 190 [24]	0.24 [24]			
Ti–TiNi on oxide	Thermal oxide	Same as above	Same as above	475 ± 20	Same as above	40 ± 12
	Ti	90 [25]	0.33 [26]	Combined metal film 270 ± 20	Combined 750 ± 100 (tensile)	
	TiNi	60 [27] 29 [28]	0.33 [28]			

stressed lower layer impervious to silicon etching, thermal oxide (SiO_2) was grown on silicon wafers (figure 2(*a*)). Thermally grown oxide on silicon has a very high compressive stress due to the differential thermal expansion of the coating and substrate as the wafers cool. Photoresist was patterned on the oxide for liftoff, and topped with sputtered chromium, nickel, titanium or other metal layer. Removal of the photoresist in acetone created a metal pattern (figure 2(*b*)) which protected the underlying oxide, while the exposed oxide was removed using a plasma etch (figure 2(*c*)). The resulting patterned bimorphs were then released from the silicon substrate by xenon difluoride (XeF_2) vapor etching (figure 2(*d*)), curling out of the wafer plane to relieve the compressive stress in the oxide. Typical values of the elastic modulus for oxide is 75 GPa and for chromium it is 140 GPa (table 1). The XeF_2 etch process is highly selective to silicon, enabling a wide range of metals and other materials to be used in the process.

Details of the fabrication steps are as follows.

3.1. Wet thermal oxide deposition

Batches of 4 inch, p-doped, 5–20 ohm cm (1 0 0) silicon wafers were coated with ∼400 nm of thermal oxide by 1 h treatment in a tube furnace at 1000 °C, with 440 sccm O_2 gas flowing into the furnace through a bubbler filled with 95 °C deionized water.

3.2. Metal patterning by liftoff

The oxidized wafers were treated with hexamethyldisilazane (HMDS) adhesion promoter, followed by coating with Shipley 1827 photoresist (Rohm and Haas Electronic Materials) at 4000 RPM for 10 s. After a 90 s hotplate solvent-removal bake at 115 °C, the photosensitized wafers were exposed to UV light through a photomask on a Karl Suss contact aligner. The photoresist was cleared from exposed areas by a 2 min development step in MF319 developer (Rohm and Haas) followed by rinsing in deionized water and drying under nitrogen gas. Wafers with patterned resist were then sputter coated with chromium–nickel–chromium (Cr–Ni–Cr), or alternatively, Ti–TiNi layers in a Technics sputtering system as follows.

Cr–Ni–Cr. For the chromium adhesion layer, sputter conditions were 120 W dc power, 30 mTorr argon chamber pressure, for 3 min. For nickel, 350 W RF power, 30 mTorr argon pressure and 5–10 min sputter time (for various thicknesses). The nickel was topped by a second Cr deposition similar to the adhesion layer to protect it from subsequent etching if needed. Combined layer thickness was measured at 160 nm (for the 5 min Ni deposition) using a Dektak profilometer.

Ti–TiNi. For the titanium adhesion layer, sputter conditions were the same as Cr above. For the TiNi, conditions were the same as Ni above, except an equiatomic TiNi target was used. 3 min nickel deposition followed by 10 min TiNi deposition resulted in a total layer thickness of 270 nm.

Following sputtering, the excess metal was removed from the unexposed resist by liftoff in acetone overnight, or within 2 h using ultrasonic agitation in acetone.

3.3. Oxide etching

The patterned metal was used as a self-mask to transfer the design into the underlying oxide. Wafers were processed in a March plasma etcher, with 240 mTorr pressure of CF_4:H_2 at a partial pressure ratio of 60:40 and a RF power of 260 W. After 10 min of etching, the 400 nm oxide was completely removed from any areas unprotected by metal.

3.4. Release by isotropic silicon etch

Bimorphs were released from the wafer by undercutting in a XeF_2 dry silicon etcher (Xactix). This isotropic etch process completely removed silicon from the underside of the oxide layer, and left a silicon cusp on the substrate at the centerline of the released structure. For 5 μm lines, the etch process required 20 or more 30 s cycles of exposure to an atmosphere of 3 Torr XeF_2 for complete release. The etch rate depends on the area of exposed silicon and will vary from pattern to pattern. However, wider lines always require more etch cycles for complete release, providing a mechanism to control the folding sequence of micro-objects based on XeF_2 etch time.

4. Discussion of material properties and predicted curvature

The properties of materials used in this paper are listed in table 1 together with calculated curvature radii from

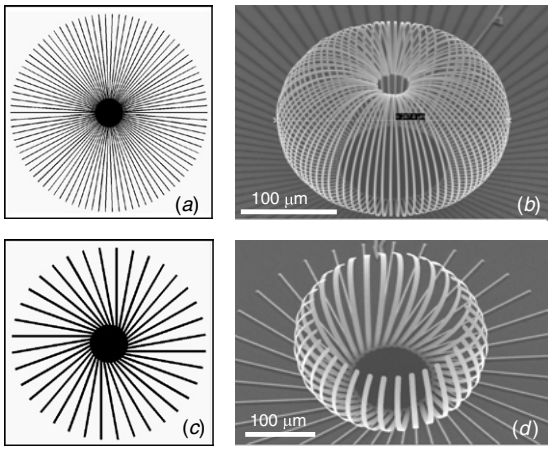

Figure 3. (*a*) Layout for toroid structure. Center anchor pad diameter 100 μm arms 300 μm long and 2 μm wide. (*b*) Released toroid with 400 nm oxide, 50–60–50 nm Cr–Ni–Cr film. Radius of curvature = 64 μm. (*c*) Layout for tilted radial structure with arms off-axis from the center. Anchor pad diameter 100 μm, arm length 200 μm, arm width 5 μm. (*d*) Released tilted structure with same materials and thicknesses.

equation (1) for both Cr–Ni–Cr devices and Ti–TiNi devices. Note that these calculations do not account for the Cr or Ti adhesion layers, instead using the Ni or TiNi biaxial elastic modulus for the entire metal film.

Strain mismatch and film thickness are far more important than elastic modulus in determining the curvature [18]. Because residual film stress is highly dependent upon processing conditions, we measured the biaxial stress σ of our oxide and metal films by profilometry of a substrate before and after film deposition. The strain mismatch required in equation (1) was then computed as

$$\varepsilon = \frac{\sigma_{\text{metal}}(1-\nu_{\text{metal}})}{E_{\text{metal}}} - \frac{\sigma_{\text{oxide}}(1-\nu_{\text{oxide}})}{E_{\text{oxide}}}. \qquad (3)$$

Values for the elastic modulus and Poisson's ratio were obtained from the literature as noted, using values reported for thin films instead of bulk materials wherever possible. Where two values appear, these were averaged for use in the calculation.

5. Results

5.1. Simple structures with two characteristic release times

The simplest structures described in this report have two characteristic line widths: one narrow width for released structures and one relatively large width to anchor the structures to the surface. Making the anchor width much greater than that of the released structures means that exact etch timing is not critical for achieving reproducible results. In scanning electron micrograph (SEM) images, we observed that features roll up along their longest dimension, as shown for the radial design in figure 3(*a*) (photomask layout) and figure 3(*b*) (SEM image) of the resulting toroid. In all SEM images, a ridge of silicon appears on the substrate at the centerline of the original two-dimensional pattern. When the lines are angled off-axis from the center of the circle, the slats of the toroid become tilted with respect to the surface (refer to figure 3(*c*), photomask layout and figure 3(*d*), SEM image). The observed 64 μm curvature radius in figure 3(*a*) is very close to the calculated radius of 64 $\pm$ 7 μm. While neighboring structures were nearly identical to each other, the observed radius varied from 60 to 100 μm across the 4 inch wafer, due to local thickness or stress variations in the sputtered metal film.

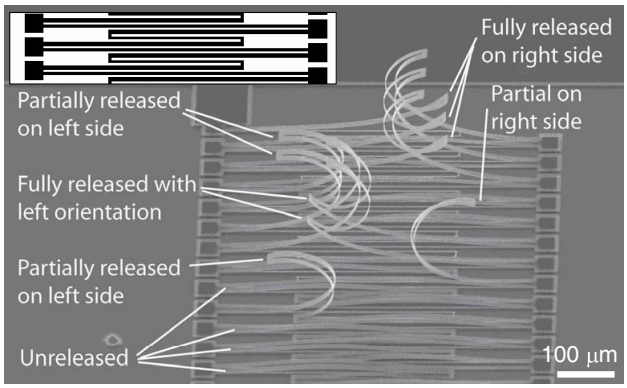

Figure 4. Inset: layout for symmetric zigzag structure. Anchor pads are 30 μm $\times$ 30 μm. Short central bar of zigzag is 5 μm wide, while long bars are 7 μm wide. Scanning electron micrograph shows arrangement of bimorphs during the release process. The release sequence is randomly determined by small differences in the widths of the pattern, and results in a left or right orientation for the completely released structures. (Oxide thickness 400 nm and Cr–Ni–Cr 50–60–50 nm.)

Because the metal layer has a thermal expansion coefficient approximately 20 times that of the oxide, these metal/oxide pop-up structures can be reversibly opened by heating; for a detailed exploration of similar structures in metal/diamond, see [13, 14].

5.2. Structures with randomly determined release times

The seemingly unpredictable folding of a 'zigzag' structure points to the importance of the release sequence in determining the final three-dimensional shape. Figure 4 (inset) shows the layout of a repeating, symmetric zigzag with anchors on each side. Due to random imperfections in the photolithography process, either the left or right bend in the zigzag is released from the surface first, as shown in the partially released structures in figure 4. After initial release, the rest of the zigzag is undercut, and the fully released structure takes on a left- or right-oriented conformation that produces a local minimum for the stored elastic energy. Continued silicon etching after this point, until only a 10 μm diameter attachment point remains at the center of the square anchor pads, does not change the left or right orientation of the structures. Although the initial pattern is symmetric, the two possible release sequences produce a set of mirror-image final structures.

5.3. Structures with engineered incremental release times

To study the interaction of structures having several incremental release steps, we created a series of nested 'V' structures with 1 μm differences in their linewidths. One type of structure had the widest line on the outside, and was

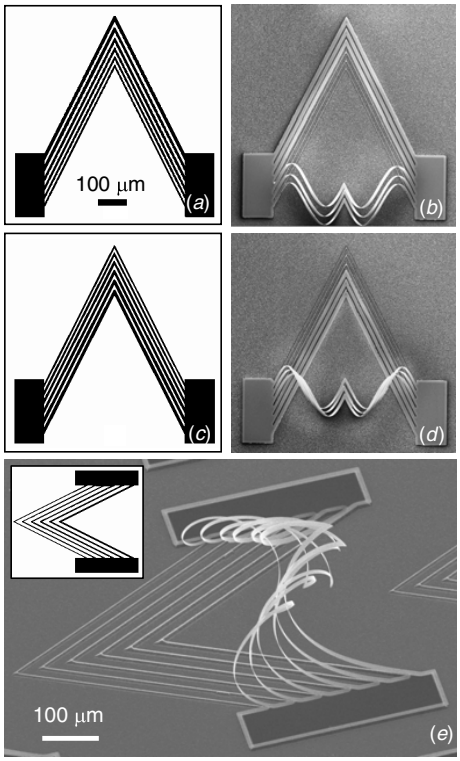

Figure 5. (*a*) Layout of untangled V-structure. Line widths range from 10 μm to 5 μm in 1 μm increments, with 5 μm spacing. (*b*) Partially released untangled V-structure, showing independent 5, 6 and 7 μm wide structures. Oxide thickness is 475 nm, Ti–TiNi thicknesses are 50 and 220 nm respectively. (*c*) Layout for tangled-V structure, with linewidth order reversed from untangled-V structure. (*d*) Partially released tangled V-structure, showing 5, 6 and 7 μm structures wrapped around each other due to release sequence. Materials and thicknesses same as (*b*). (*e*) Side view of a fully released tangled-V structure with 15 μm spacing between lines (inset shows layout). Oxide thickness is 400 nm and Cr–Ni–Cr thicknesses are 50–60–50 nm.

expected to produce independent structures. The other type had the widest line on the inside, and was expected to tangle as the narrowest V released first and curled over the still-unreleased lines. Figure 5(*a*) shows the layout for the untangled V, and figure 5(*b*) is a scanning electron micrograph above this structure after the three narrowest lines have released. Figure 5(*c*) shows the 'tangled-V' layout, and figure 5(*d*) a top view after the first three lines have released. In the untangled structure, the lines remain independent, while in the tangled version, the lines have wrapped around one another. Figures 5(*b*) and (*d*) use Ti–TiNi rather than the previous Cr–Ni–Cr metal films. The Ti–TiNi devices are expected to have a smaller radius of curvature (40 $\pm$ 12 μm versus 64 $\pm$ 7 for Cr–Ni–Cr), but the curvature equation (1) does not apply directly to these constrained structures. Figure 5(*e*) is a side view of another tangled structure made from Cr–Ni–Cr, with 15 instead of 5 μm spacing between the lines, showing the nature of the overlap that is initiated by narrow lines curling over wider lines before the wider lines are released, as well as a qualitatively larger radius of curvature than similar Ti–TiNi structures. Simply reversing the order of the linewidths has created dramatically different final structures.

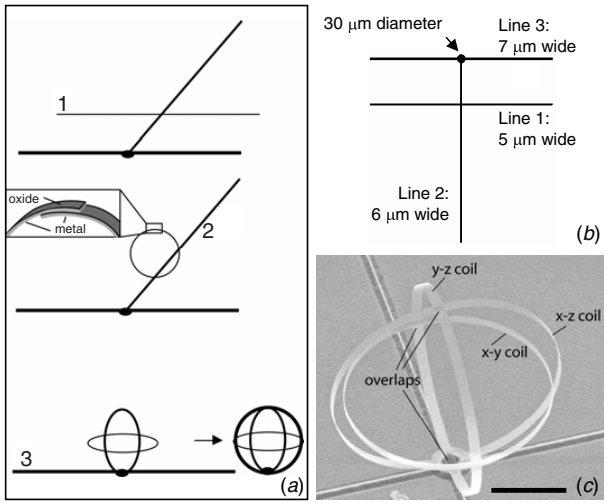

Figure 6. (*a*) Three-step fabrication sequence for a three-axis loop structure from a single photomask. Loop 1 forms and is lifted up by formation of loop 2, after which loop 3 wraps around the previously formed loops. (*b*) Layout for the structure consists of 5, 6 and 7 μm lines connected to a 30 μm diameter pad. Lines are 628 μm long, for an anticipated ~100 μm coil radius. (*c*) The finished structure showing coils in *x*–*y*, *x*–*z* and *y*–*z* planes. Scale bar is 50 μm and coil radius is 90 μm. Oxide thickness is 400 nm and Cr–Ni–Cr thicknesses are 50–60–50 nm.

5.4. Structure with carefully controlled release sequence

A three-step sequence for fabricating a multiaxis loop structure is illustrated in figure 6(*a*). The layout for this sequence is shown in figure 6(*b*), where the expected 100 μm coil radius has been used to design three single-turn loops which will orient themselves along three orthogonal planes when released. The 5 μm wide coil releases first, followed by the 6 and 7 μm coils. Figure 6(*c*) shows the resulting structure, with overlaps at the ends of the three loops.

6. Conclusions

The metal-oxide bimorph release process detailed here can produce highly uniform and predictable structures, as long as there is good control over film stress and thickness, and the effects of the folding sequence are considered during the design phase. Careful control of the folding sequence adds the ability to make sophisticated multi-axis structures from a single photomask. We have reliably used width differences of 1 μm, readily accessible by contact photolithography, to control the release order. This may be considered an upper limit for the linewidth difference needed for reproducible folding order. Higher resolution patterning will enable investigations into the lower limit of this sequential assembly technique.

The randomly released zigzag structures we observed in figure 4 may suggest a path to bistable structures with applications as latching mechanical actuators, since these have found two mirror-image energy-minimizing configurations. In this application, the dimensions and materials must be optimized to avoid permanent deformation in the initial configuration.

Tangled V-structures in figure 5 may find applications as temporary or permanent clips to join micro- or nanostructures

together on a substrate. Since these structures have contact pads at each end, they may be thermally actuated to open and close by Joule heating.

The multi-axis coils illustrated in figure 6 have potential applications as isotropic electromagnetic resonators and antenna elements, and will retain their shape even if detached completely from the wafer as separate particles. Such particles, if designed to have a narrow electrical resonance, may function as microtaggants for electromagnetic identification, or polarization-insensitive antenna array elements.

When designing such multi-step folding structures, it becomes clear that several different patterns may lead to a similar final shape; for instance, in figure 6 the narrow 5 μm crossbar could have been placed near the other end of the 6 μm line to produce a horizontal coil. In this case, the optimal two-dimensional pattern might be the one that maximizes packing density on the wafer, since neighboring structures must not touch or cross in the original layout. If routing problems become difficult, it is also possible to integrate additional metallization and low-temperature oxide/silicon coating steps before the structures are released. Doing so can enable structures that cross, and structures with different curvature radii on a single wafer, moving beyond the single-photomask process described here.

Acknowledgments

Microfabrication was supported by Mark Crain, Ana Kieswetter, Joseph Lake, Dr Julia Aebersold, Don Yeager and John Henson in the University of Louisville cleanroom. We would also like to acknowledge Dr Mehdi Yazdanpanah for assistance in testing devices, Dr Robert Cohn for technical discussions and David Springer at Xactix for support with XeF_2 etching.

References

[1] Prinz V Ya, Seleznev V A, Gutakovsky A K, Chehovskiy A V, Preobrazhenskii V V, Putyato M A and Gavrilova T A 2000 Free-standing and overgrown InGaAs/GaAs nanotubes, nanohelices and their arrays *Physica* E **6** 828

[2] Schmidt O G and Eberl K 2001 Nanotechnology—thin solid films roll up into nanotubes *Nature* **410** 168

[3] Huang M N, Boone L, Roberts M, Savage D E, Lagally M G, Shaji N, Qiu H, Blick R, Nairn J A and Liu F 2005 Nanomechanical architecture of strained bilayer thin films: from design principles to experimental fabrication *Adv. Mater.* **17** 2860

[4] Schmidt O G and Jin-Phillipp N Y 2001 Free-standing SiGe-based nanopipelines on Si (0 0 1) substrates *Appl. Phys. Lett.* **78** 3310

[5] Vaccaro P O, Kubota K and Aida T 2001 Strain-driven self-positioning of micromachined structures *Appl. Phys. Lett.* **78** 2852–4

[6] Schumacher O, Mendach S, Welsch H, Schramm A, Heyn Ch and Hansen W 2005 Lithographically defined metal-semiconductor-hybrid nanoscrolls *Appl. Phys. Lett.* **86** 143109

[7] Zanardi Ocampo J M, Vaccaro P O, Fleischmann T, Wang T-S, Kubota K and Aida T 2003 Optical actuation of micromirrors fabricated by the micro-origami technique *Appl. Phys. Lett.* **83** 3647–9

[8] Vaccaro P O, Kubota K, Fleischmann T, Saravanan S and Aida T 2003 Valley-fold and mountain-fold in the micro-origami technique *Microelectronics J.* **34** 447–9

[9] Lee C, Lai Y J, Wu C-Y, Yeh J A and Huang R-S 2005 Feasibility study of self-assembly mechanism for variable optical attenuator *J. Micromech. Microeng.* **15** 55–62

[10] Varob'ev A, Vaccaro P, Kubota K, Saravanan S and Aida T 2003 Array of micromachined components fabricated using 'micro-origami' method *Japan. J. Appl. Phys.* **1** 4024–6

[11] Tsai J T H, Teo K B K and Milne W I 2002 Approach for a self-assembled thin film edge field emitter *J. Vac. Sci. Technol. B* **20** 1–4

[12] Zhou J W L, Chan H-Y, To T K H, Lai K W C and Li W J 2004 Polymer MEMS actuators for underwater micromanipulation *IEEE/ASME Trans. Mechatronics* **9** 334–42

[13] Luo J K, He J H, Fu Y Q, Flewitt A J, Spearing S M, Fleck N A and Milne W I 2005 Fabrication and characterization of diamond-like carbon/Ni bimorph normally closed microcages *J. Micromech. Microeng.* **15** 1406–13

[14] Luo J K, Huang R, He J H, Fu Y Q, Flewitt A J, Spearing S M, Fleck N A and Milne W I 2006 Modelling and fabrication of low operation temperature microcages with a polymer/metal/DLC trilayer structure *Sensors Actuators* A **132** 346–53

[15] Suh J W, Darling R B, Bohringer K-F, Donald B R, Baltes H and Kovacs G T A 1999 CMOS integrated ciliary actuator array as a general-purpose micromanipulation tool for small objects *J. Microelectromech. Syst.* **8** 483

[16] Chang C, Chiang C-F, Liu C-H and Liu C-H 2005 A lobster-sniffing-inspired method for micro-objects manipulation using electrostatic micro-actuators *J. Micromech. Microeng.* **15** 812–21

[17] Johnstone R W, Sameoto D and Parameswaran M 2006 Non-uniform residual stresses for parallel assembly of out-of-plane surface micromachined structures *J. Micromech. Microeng.* **16** N17–22

[18] Timoshenko S 1925 Analysis of bi-metal thermostats *J. Opt. Soc. Am.* **11** 233–55

[19] Krulevitch P and Johnson G C 1998 Curvature of a cantilever beam subjected to an equi-biaxial bending moment *Mater. Res. Soc. Symp. Proc.* **518** 67–72

[20] Weast R C (ed) 1971 *Handbook of Chemistry and Physics* 51st edn (Cleveland, OH: CRC Press)

[21] Riethmuller W and Benelke W 1988 Thermally excited silicon microactuators *IEEE Trans Electron Devices* **35** 758–63

[22] Zhao J-H, Ryan T, Ho P S, McKerrow A J and Shih W-Y 1999 Measurement of elastic modulus, Poisson ratio, and coefficient of thermal expansion of on-wafer submicron films *J. Appl. Phys.* **85** 6421–4

[23] Lintmyer J, Martin N, Chappe J-M, Takadoum J and Delobelle P 2006 Modeling of Young's modulus, hardness, and stiffness of chromium zigzag multilayers sputter deposited *Thin Solid Films* **503** 177–89

[24] Namazu T and Inoue S 2007 Characterization of single crystal silicon and electroplated Ni films by uniaxial tensile test with in-situ x-ray diffraction measurement *Fat. Frac. Eng. Mater. Struct.* **30** 13–20

[25] Tsuchiya T, Hirata M and Chiba N 2005 Young's modulus, fracture strain, and tensile strength of sputtered titanium thin films *Thin Solid Films* **484** 245–50

[26] Moroi H H, Okimoto K, Moroi R and Terada Y 1993 Numeric approach to the biomechanical analysis of thermal effects in coated implants *Int. J. Prosthodont* **6** 564–72

[27] Fu Y Q, Huang W M, Du H J, Huang X, Tan J P and Gao X Y 2001 Characterization of TiNi shape memory alloy thin films for MEMS applications *Surf. Coat. Technol.* **145** 107–12

[28] Fu Y Q, Zhang S, Wu M J, Huang W M, Du H J, Luo J K, Flewitt A J and Milne W I 2006 On the lower thickness boundary of sputtered TiNi films for shape memory application *Thin Solid Films* **515** 80–6